Edge-Localized-Mode–Induced Transport of Impurity Density, Energy, and Momentum

M. R. Wade,[1,*] K. H. Burrell,[2] A. W. Leonard,[2] T. H. Osborne,[2] and P. B. Snyder[2]

[1]*Oak Ridge National Laboratory, Oak Ridge, Tennessee, 37831 USA*

[2]*General Atomics, P.O. Box 85608, San Diego, California, 92186-5608 USA*

(Received 28 May 2004; published 7 June 2005)

High temporal and spatial resolution measurements of impurity dynamics associated with an edge-localized mode (ELM) indicate that the ELM perturbation consists of two distinct parts: a rapid (<300 μs) expulsion of impurity density at the time of the instability followed by a slower time scale (<1 ms) decrease in the ion temperature. While the density perturbation remains nearly constant over a wide range of plasma collisionality, the temperature perturbation decreases as the collisionality increases. Analysis of the radial electric field E_r evolution indicates that the E_r well normally present in H-mode plasmas is modified strongly by the ELM and that the size of the temperature perturbation is correlated with the associated change in the $E \times B$ shear.

DOI: 10.1103/PhysRevLett.94.225001 PACS numbers: 52.30.Cv, 52.25.Fi, 52.25.Vy, 52.55.Fa

Since the discovery of the H mode [1], significant research, both experimental and theoretical, has focused on characterizing the dynamics of commonly observed edge instabilities known as edge-localized modes (ELMs) [2]. While this characterization is far from complete, it is clear that ELMs pose a serious technical challenge to the design of future burning devices due to the high transient heat and particle fluxes on plasma facing surfaces [3]. While recent studies suggest that these ELMs are initially triggered by peeling-ballooning instabilities originating near the plasma edge [4], a complete description of the ELM instability and its associated transport effects is still lacking. In particular, ion and impurity transport during the ELM cycle have not been studied in detail due to the high temporal and spatial resolution that is required to resolve the profile response adequately. The results reported in this Letter are a first step towards bridging this gap and suggests that the response of E_r to the ELM event plays an important role in the impurity transport associated with the ELM.

The studies discussed here focus on the dynamics of a particular class of ELMs, known as type-I ELMs [2], which are believed to be initially triggered by ideal magnetohydrodynamic (MHD) instabilities of moderate toroidal mode number $n(\sim 5$–$20)$ that originate near the plasma edge and have limited radial extent [4]. This class of instabilities, known collectively as peeling-ballooning modes, can be driven unstable by either the edge pressure gradient (i.e., ballooning) or edge current density (i.e., peeling). Previous studies have shown that the electron density and temperature profiles in the edge crash on a very fast time scale (~ 100–300 μs) following a type-I ELM [5,6]. These studies have consistently shown that the density and temperature perturbation caused by the ELM is localized near the plasma edge. In some cases, the observed perturbations are in qualitative agreement with that expected from peeling and ballooning theory. The studies discussed here take advantage of recent upgrades to the DIII-D charge-exchange recombination (CER) spectroscopy system [7] to allow spectral framing times as low as 274 μs. This system consists of 48 channels that measure charge-exchange emission from the interaction of fully stripped impurity atoms and energetic neutrals [8] injected by three separate neutral beam sources. The $C^{+5} n = 8 - 7$ transition at 5290 A is used to provide a direct measurement of the C^{+6} density, temperature, and rotation velocity. The spatial resolution of this system at the plasma edge (~ 3 mm for impurity density n_{C+6} and temperature, ~ 6 mm for toroidal v_ϕ and poloidal rotation v_θ) is sufficient to provide detailed information on the profiles in the high gradient region near the edge of an H-mode plasma. Since the ion-impurity energy equilibration time [defined as $\tau_{i,Z}^{\mathrm{eq}} \approx 2.4 \times 10^{-6} T_D^{3/2}\,(\mathrm{keV})/n_D(10^{19}\,\mathrm{m}^{-3})$ where n_D and T_D are the deuteron density and temperature, respectively] is <10 μs for typical edge plasma conditions, $T_{C+6} \approx T_D$ throughout this region. We refer to this quantity as the ion temperature T_i throughout this Letter.

An example of the quality of data available from this system is shown in Fig. 1, in which the temporal evolution of n_{C+6}, T_i, v_{tor}, and v_{pol} deduced by CER spectroscopy for several radial locations during a series of ELM events is shown. From Fig. 1, it is clear that each ELM causes a significant decrease in n_{C+6}, T_i, v_{tor}, and v_{pol} on a very short time scale on all channels viewing within 8 cm of the plasma separatrix location (denoted by R_{sep}). Since these analyzed quantities are deduced from a spectrum that represents an average of the spectral emission during an integration period, we have chosen to denote the time for the measurement in analysis (and in Fig. 1) as the centroid of the integration period over which the spectral data were obtained. The decrease in n_{C+6} occurs in no more than one integration period (550 μs), and possibly less. At the fastest time resolution available to date of 3.7 kHz (270 μs integration time), the expulsion is also observed to occur in less than one integration period, indicating the expulsion occurs in less than 300 μs. The radial extent of the expulsion in terms of the normalized radius is from $0.6 < \hat{\rho} < 1.0$ where $\hat{\rho}$ is the normalized plasma radius.

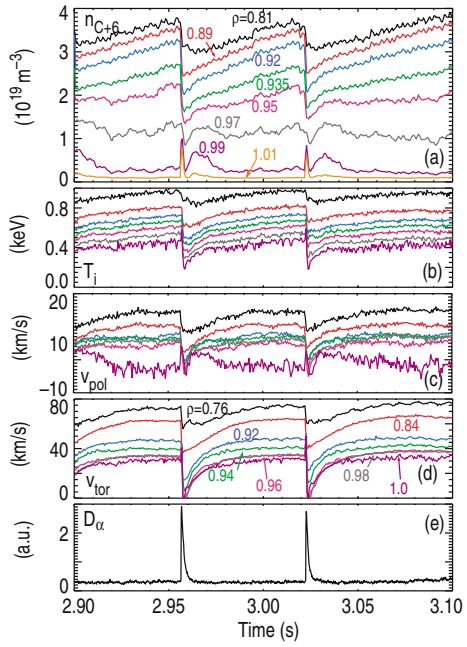

FIG. 1 (color). Temporal evolution of edge impurity profiles during a set of ELM cycles: (a) n_{C+6}; (b) T_i; (c) $v_{\rm pol}$; (d) $v_{\rm tor}$ at various normalized radii ρ along the outboard midplane; (e) midplane D_α signal. The color scheme is the same for (a), (b), and (c).

The observed changes in v_ϕ and $v_{\rm pol}$ are suggestive of a change in the radial electric field E_r, whose relationship to the rotation velocities is given by the radial force balance equation: $E_r = (Z_{\rm j} e n_{\rm j})^{-1} \nabla p_{\rm j} - v_{\theta {\rm j}} B_\phi + v_{\phi {\rm j}} B_\theta$. Here, $Z_{\rm j}$ is the ion charge, $n_{\rm j}$ is the ion density, e is the magnitude of the electron charge, $p_{\rm j} = n_{\rm j} T_{\rm j}$ is the ion pressure, $v_{\theta {\rm j}}$ and v_ϕ are, respectively, the poloidal and toroidal rotation velocities, and $B_{\theta {\rm j}}$ and $B_{\phi {\rm j}}$ are, respectively, the poloidal and toroidal magnetic fields.

To improve the statistics in the analysis of the time evolution of the ELM dynamics, a mapping technique has been used that maps data from a set of reproducible ELM cycles onto a single time base relative to the time of the closest ELM. The time for the ELM event is taken to be the time of the maximum amplitude in the midplane D_α signal to avoid any issues related to divertor recycling time scales. Using this technique, the overall perturbation in the various observables by the ELM can be determined by separately fitting the pre-ELM and post-ELM phases with a linear function. The pre-ELM and post-ELM values are then taken as the value of the respective fits at -1 and 1 ms, respectively. The relative perturbation is then given by $\delta \hat{f} = \Delta f / f_{\rm pre-ELM}$, where Δf represents the measured difference between the pre-ELM and post-ELM values of observable f.

The perturbations determined in this manner for both n_{C+6} and T_i for a density scan at fixed input power and magnetic configuration are shown in Figs. 2(a) and 2(b). It is evident from Fig. 2 that $\delta \hat{n}_{C+6}$ remains essentially constant as the density is varied, while $\delta \hat{T}_i$ decreases systematically as the density is increased. This is consistent with previous studies of the variation of the n_e and T_e perturbations with plasma density [5]. Remarkably, within the data set described here, the overall electron and impurity perturbations are quite similar (i.e., $\delta \hat{n}_{C+6} \approx \delta \hat{n}_e$ and $\delta \hat{T}_i \approx \delta \hat{T}_e$) over the entire density range. In conjunction with the constraint of quasineutrality, this implies that the overall response of all species is also quite similar. The robustness of this result over a wide range of plasma conditions is highly suggestive that the fundamental transport process at the ELM event involves $E \times B$ transport that is independent of particle charge or mass.

Further analysis of the response of the various observables to the ELM event suggests that the mechanisms contributing to the magnitude of $\delta \hat{n}_{C+6}$ and $\delta \hat{T}_i$ may be different. This is most evident when looking at the details of the dynamics associated with the ELM event. Using the same time-mapping technique as described earlier, a detailed time history of the various observables can be constructed by applying a 0.5 ms boxcar average to the time-mapped quantities. The result of such analysis for the low density case of the density scan discussed above is shown in Fig. 3. As noted before, events occurring on times shorter than a framing time are still not discernible via this technique since each frame's spectrum averages over the entire framing time. Hence, the timing (both in terms of time relative to the ELM and the time scale) of changes induced by the ELM can be resolved only to the data framing time (in this case, 0.552 ms). Nevertheless, the decrease in n_{C+6} and the increase of T_i near the time of the ELM event are real. The time scale for the decrease in n_{C+6} is the shortest for those channels in the region $0.9 \leq \hat{\rho} \leq 0.96$, with little or no change seen on channels inside this region. The region of the short-term increase in T_i is shifted slightly outward from the region of density loss. This

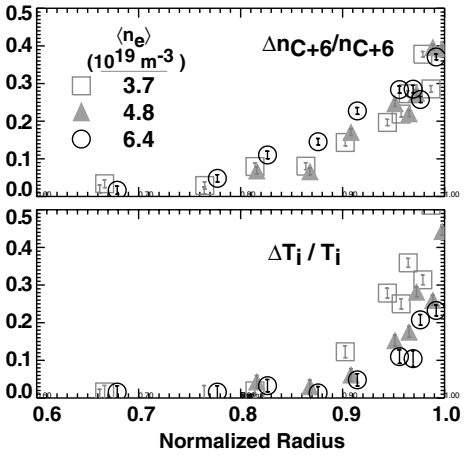

FIG. 2. Radial perturbation of (a) n_{C+6} and (b) T_i during a density scan under otherwise similar conditions.

observation is qualitatively consistent with a rapid convective energy loss that transports plasma from a radial location inside the measurement location, where the plasma has higher T_i. The brief increase in T_i is followed by a decrease that occurs on an approximately 1 ms time scale. The time scale of this decrease and its delay relative to the ELM and the initial density decrease suggest that this may be a response of the transport properties to the ELM event rather than transport caused directly by the MHD instability itself.

As noted previously, the measured changes in $v_{\rm tor}$ and $v_{\rm pol}$ at the ELM event are suggestive that the ELM causes rapid changes in E_r. The evolution of the E_r profile inferred from the measured n_{C+6}, T_i, $v_{\rm tor}$, and $v_{\rm pol}$ is shown in Fig. 3(d). Note that the variation of E_r throughout this entire region is dominated by the $v \times B$ contribution to E_r with the ∇p term only contributing modestly very close to the separatrix. Just before the ELM event ($t - t_{\rm ELM} = -1$ ms), there is significant shear in the E_r profile throughout the entire edge region with a region within 2–3 cm of the plasma edge in which $E_r < 0$ everywhere. Though not shown in Fig. 3(d), $E_r \sim 0$ at the separatrix location, forming a deep well in E_r just inside the separatrix. In this case, the E_r well is obliterated by the ELM event ($t - t_{\rm ELM} = 0$ ms) and $E_r \sim 0$ within 2–3 cm of the plasma edge immediately after the ELM. Inside this region, E_r decreases modestly at the time of the ELM, resulting in a reduction in the E_r shear across the entire edge region from its pre-ELM state.

Previous theoretical and experimental studies have shown the importance of E_r shear on the underlying transport properties [9]. These studies have shown that the $E \times B$ shearing rate [defined as $\omega_{E\times B} = (R^2 B_\theta^2/B) \times \partial(E_r/RB_\theta)/\partial\psi$ where B is the magnitude of the magnetic field and ψ is the toroidal magnetic flux] can cause decorrelation of the underlying turbulence, leading to a reduction in the turbulence-driven transport. Using the data from the density scan of Fig. 2, it has been found that the magnitude of the change in $\omega_{E\times B}$ associated with the ELM is dependent on the plasma density. This is exemplified in Fig. 4. In this figure, $\omega_{E\times B}^{\rm ped}$ is the overall shearing rate from the top of the pedestal to the separatrix as deduced from measurements of E_r at these locations. The change in $\omega_{E\times B}^{\rm ped}$ caused by the ELM is observed to be the largest at the lowest density, with only a small change in $\omega_{E\times B}^{\rm ped}$ observed at high density. Note that the main difference in the evolution of the various cases is the magnitude of $\omega_{E\times B}^{\rm ped}$ leading up to the ELM. In fact, the minimum value of $\omega_{E\times B}^{\rm ped}$ (obtained just after the ELM) in the low density case is as large as the maximum value of $\omega_{E\times B}^{\rm ped}$ (obtained just before the ELM) in the high density case.

From the basic theory of $E \times B$ shear reduction of turbulence transport, one would expect the observed differences in the evolution of $\omega_{E\times B}$ to affect transport also. Note that theory predicts the strength of $E \times B$ shear decorrelation of electrostatic turbulence to scale as $\omega_{E\times B}^2$ [9]. The dependence of the conductive ($\Delta W_{{\rm cond},Z}$), convective ($\Delta W_{{\rm conv},Z}$), and total ($\Delta W_{{\rm tot},Z}$) energy losses caused by the ELM on the magnitude of the change in $(\omega_{E\times B}^{\rm ped})^2$ is shown in Fig. 5. Here, $\Delta W_{{\rm cond},Z} = 3/2 \int \bar{n}_{C+6} \Delta T_i dV$, $\Delta W_{{\rm conv},Z} = 3/2 \int \Delta \bar{n}_{C+6} T_i dV$, and $\Delta W_{{\rm tot},Z} = 3/2 \int \Delta(\bar{n}_{C+6} T_i) dV$, where $\bar{f}$ is the average of the pre-ELM and post-ELM values of observable f and the integral extends over the region $0.6 \le \hat{\rho} \le 1$. Constructed in this way, $\Delta W_{{\rm conv},Z}$ and $\Delta W_{{\rm cond},Z}$ are primarily reflective of the density and temperature perturbations, respectively. A direct correlation is observed between the degree to which $\omega_{E\times B}^2$ changes across the ELM and the conductive energy loss associated with the ELM. The nearly linear correlation between $\Delta W_{{\rm cond},Z}$ and $\Delta(\omega_{E\times B}^{\rm ped})^2$ suggests that the ELM-induced change in E_r shear is playing a key role

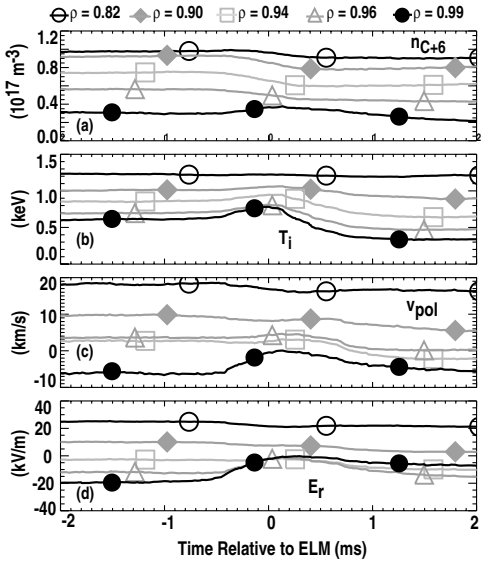

FIG. 3. Evolution of (a) n_{C+6}, (b) T_i, (c) $v_{\rm pol}$, and (d) E_r relative to the ELM event for the low density case in Fig. 2 constructed by the technique described in the text.

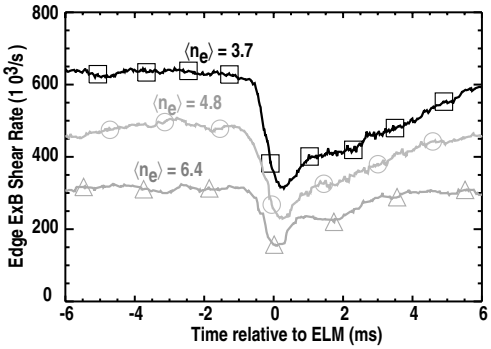

FIG. 4. Evolution of $\omega_{E\times B}^{\rm ped}$ with respect to the ELM event for various cases from the density scan of Fig. 2. Density values are in 10^{19} m^{-3}.

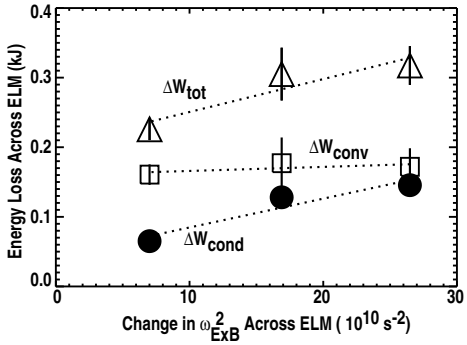

FIG. 5. Measured change in the conductive (closed circles), convective (open squares), and total (open triangles) impurity energy losses versus the change in $(\omega^{\rm ped}_{E\times B})^2$ across an ELM.

in the measured temperature drop across the ELM event. In contrast, $\Delta W_{{\rm conv},Z}$ shows little variation with $\Delta(\omega^{\rm ped}_{E\times B})^2$, indicating the density decrease across the ELM event is not strongly affected by the changes in the E_r shear. While the correlation between $\Delta W_{{\rm cond},Z}$ and $\Delta(\omega^{\rm ped}_{E\times B})^2$ is highly suggestive that the modification in the $E\times B$ shear is playing a role in the ELM-induced conductive transport, it is difficult to quantify the role of the $E\times B$ shear in the observed changes due to the complex interaction of turbulence drive and suppression mechanisms in the high gradient region at the edge. In fact, the problem is of such complexity that theory-based predictive models of edge transport are still in the development phase. As these models become available, more detailed tests will be possible.

The above observations suggest that the overall response of the impurity profiles to the ELM event is made up of two distinct parts: a rapid, convective expulsion of plasma that is relatively independent of plasma density, followed by cross-field transport of energy associated with a change in the transport properties of the edge plasma. In many respects, the overall effect of an ELM on the electron profiles appears to be quite similar to that on the impurities. The observation that the overall perturbation (i.e., the net relative change) caused by the ELM not only to n_{C+6} and n_e but also to T_i and T_e is nearly identical over a wide range in plasma conditions suggests that a common process is governing the response of the respective profiles. Unfortunately, a complete data set with time-resolved measurements of each of these quantities is not yet available on DIII-D, hence a detailed comparison of the time response of the various species is not presently possible. The limited data set that is available suggests a rapid (<300 μs), convective expulsion of electron density by the ELM [10], very similar to that seen for the impurities. Measurements of the electron temperature response on Joint European Torus via electron cyclotron emission suggest a similar, rapid decrease [11]. Yet, there are some cases in DIII-D in which the temperature decrease occurs on a longer ($\sim$1 ms) time scale. Improved time and spatial resolution of the electron response simultaneous with the impurity response should help clarify this issue.

In conclusion, measurements of the edge profile dynamics during an ELM cycle suggest that the ELM event causes a rapid (<300 μs), localized expulsion of impurity density, energy, and momentum from the edge plasma. In addition, the E_r well normally observed in H-mode plasmas is modified strongly by the ELM with the relative change decreasing as the plasma density increases. The overall impact of the ELM event is observed to be similar for the impurities and electrons over a wide range in plasma conditions, suggesting a common process governing the transport of the various species. Analysis suggests that the ELM-induced impurity transport is due to two distinct effects: a rapid, convective expulsion of plasma that is relatively independent of plasma density and increased diffusive energy transport due to the obliteration of the E_r well. This multistep transport process suggests the ELM-induced transport is different from that expected from linear, peeling-ballooning theory and will require nonlinear, dynamical models to describe. Such dynamical models in which a MHD event leads to changes in plasma transport have been proposed previously [12,13]. These high spatial and temporal resolution measurements should allow development of more detailed dynamical models capable of handling both the MHD-driven and turbulence-driven transport associated with the ELM.

This work was supported by the U.S. Department of Energy under DE-AC05-00OR22725 and DE-FC02-04ER54698.

*Corresponding author.
Electronic address: wade@fusion.gat.com

[1] F. Wagner *et al.*, Phys. Rev. Lett. **49**, 1408 (1982).
[2] H. Zohm, Plasma Phys. Controlled Fusion **38**, 1213 (1996).
[3] A. Loarte *et al.*, Plasma Phys. Controlled Fusion **45**, 1549 (2003).
[4] P. B. Snyder *et al.*, Phys. Plasmas **9**, 2037 (2002).
[5] A. W. Leonard *et al.*, Phys. Plasmas **10**, 1765 (2003).
[6] A. Loarte *et al.*, Phys. Plasmas **11**, 2668 (2004).
[7] K. H. Burrell *et al.*, Rev. Sci. Instrum. **75**, 3455 (2004).
[8] R. C. Isler, Plasma Phys. Controlled Fusion **36**, 171 (1994).
[9] K. H. Burrell *et al.*, Phys. Plasmas **4**, 1499 (1997).
[10] L. Zeng *et al.*, Rev. Sci. Instrum. **74**, 1530 (2003).
[11] A. Loarte *et al.*, Plasma Phys. Controlled Fusion **44**, 1815 (2002).
[12] V. B. Lebedev *et al.*, Phys. Plasmas **2**, 3345 (1995).
[13] J.-S. Lonnroth *et al.*, Plasma Phys. Controlled Fusion **46**, 1197 (2004).